Electronic Supplementary Material (ESI) for Journal of Materials Chemistry C.

Supporting information

Flexible and High-Performance Electrochromic Smart Window Produced by $WO_3/Ti_3C_2T_x$ MXene Hybrids

Van-Tam Nguyen [a,b,#], *Bok Ki Min* [a,#], *Seong K. Kim* [c], *Yoonsik Yi* [a], *and Choon-Gi Choi* [a,b,*]

[a] Graphene Research Team, ICT Creative Research Lab., Electronics and Telecommunications Research Institute (ETRI), 218 Gajeong-ro, Yuseong-gu, Daejeon 34129, Republic of Korea.

[b] School of ETRI (ICT-Advanced Device Technology), University of Science and Technology (UST), Daejeon 34113, Republic of Korea.

[c] Department of Advanced Materials and Chemical Engineering, Hannam University, Daejeon 34430, Republic of Korea.

* Corresponding author. Tel: +82 42 860 6834. E-mail: cgchoi@etri.re.kr

[#]V.-T. Nguyen and B. K. Min contributed equally to this work

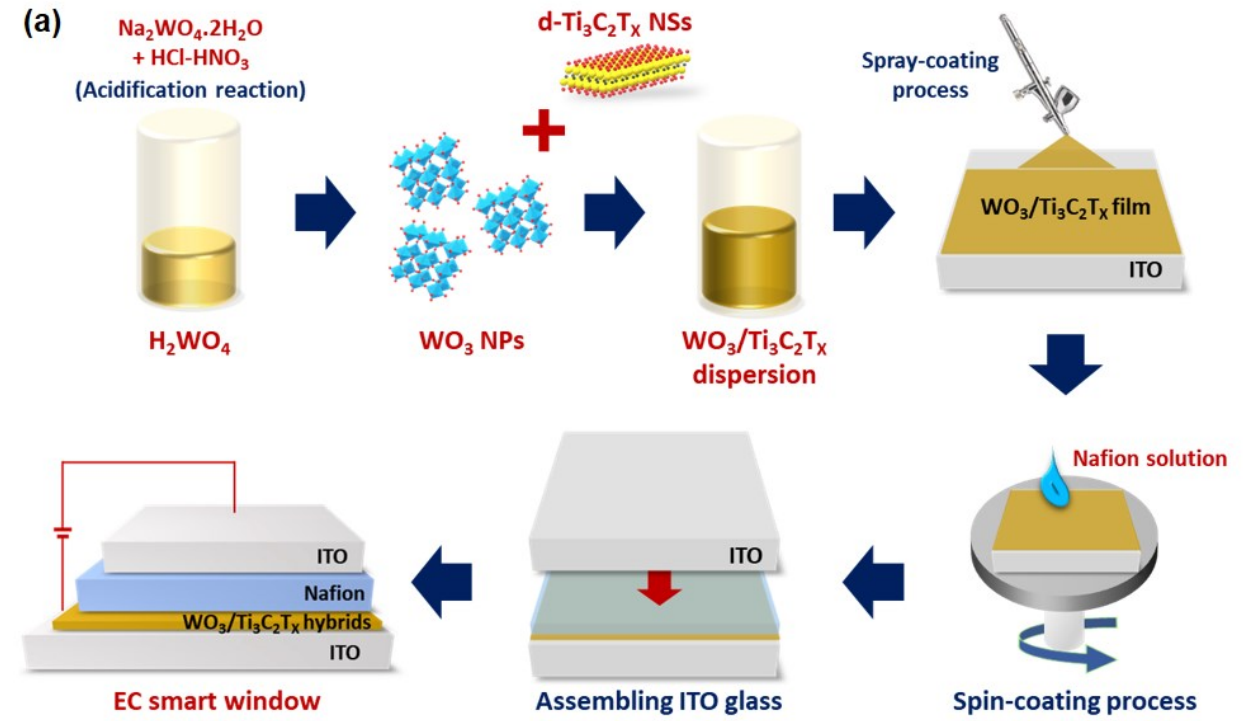

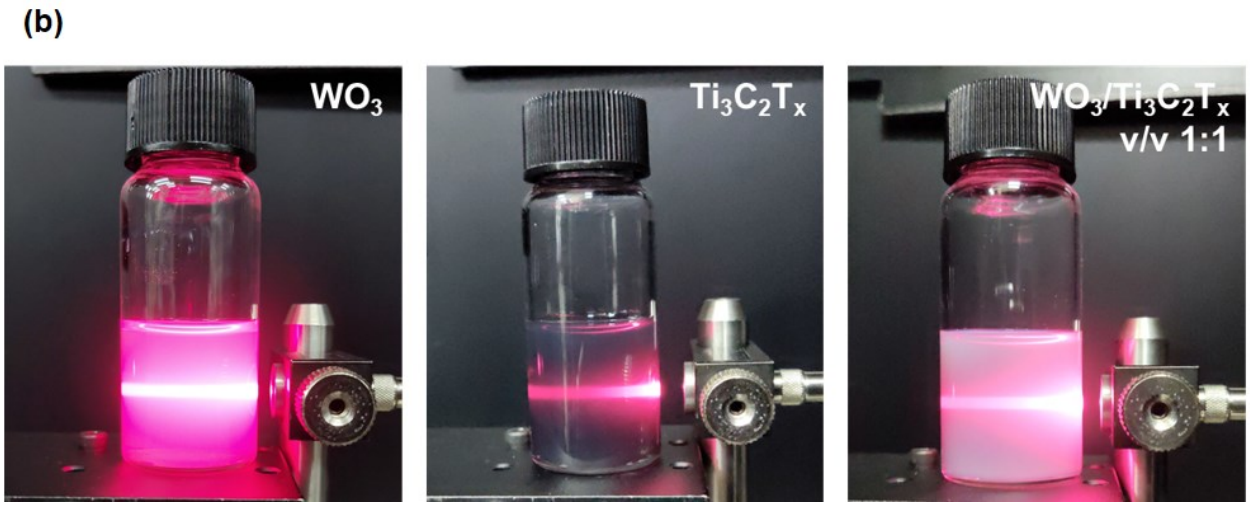

Fig. S1 (a) Schematic illustration of the fabrication procedure for electrochromic smart windows based on $WO_3/Ti_3C_2T_x$ hybrids, (b) Tyndall effect images of WO_3, $Ti_3C_2T_x$ and $WO_3/Ti_3C_2T_x$ v/v 1:1 colloid.

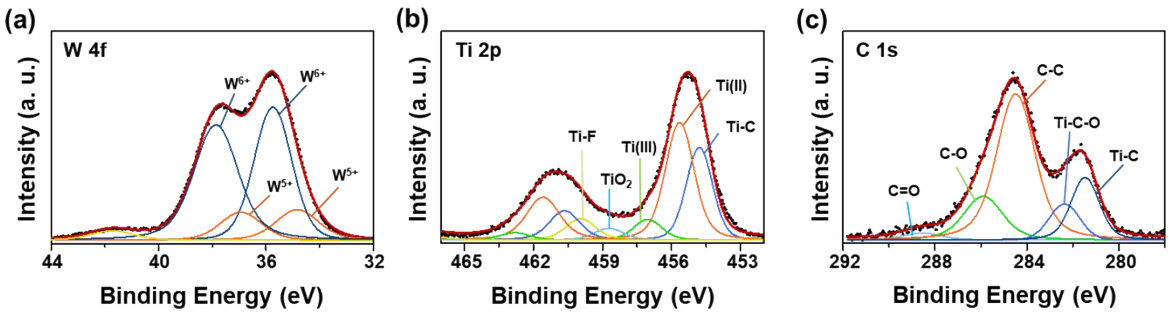

Fig. S2 XPS spectra of (a) W 4f core level, (b) Ti 2p core level, and (c) C 1s core level for $WO_3/Ti_3C_2T_x$ hybrids.

Figure S2 includes the XPS core-level spectra of each element including W 4f, Ti 2p, and C 1s for $WO_3/Ti_3C_2T_x$ hybrids. W 4f core-level spectrum shows a double peak at binding energies of 35.69 eV and 37.8 eV, attributed to W $4f_{7/2}$ and W $4f_{5/2}$, respectively (Figure S2a). These peaks are illustrative a 6+ oxidation state of W in WO_3.[1] The small peaks in at binding energy of 34.8 eV, 36.9 eV, and 41.15 eV are ascribed to a 5+ oxidation state of W in WO_3. The presence of W^{5+} state, corresponding to the cations in the non-stoichiometric WO_x along with the shear plane structure, confirms the formation of not only stoichiometric WO_3 but also non-stoichiometric WO_x. Figure S2b shows the Ti 2p core-level for the $WO_3/Ti_3C_2T_x$ hybrids. It was deconvoluted into the components corresponding to Ti–C, Ti (Ⅱ), Ti (Ⅲ), Ti(Ⅳ)–TiO_2, and Ti–F peak.[2-4] In the Ti $2p_{3/2}$ level, each component was positioned at binding energies of 454.8, 455.7, 457, 458.7, and 459.9 eV, respectively. The presence of Ti(Ⅳ)-TiO_2 and Ti-F is attributed by the terminal groups during the removal process of Al from the Ti_3AlC_2 MAX phase. From C 1s core level of $WO_3/Ti_3C_2T_x$ hybrids (Figure S2c), the spectra have two significant peaks corresponding to Ti–C and C–C bonding that are located at 281.8 and 284.7 eV, respectively.[5,6] Besides, peaks related to C=O, C–OH, and C–O–Ti bonding indicate the presence of functional groups.

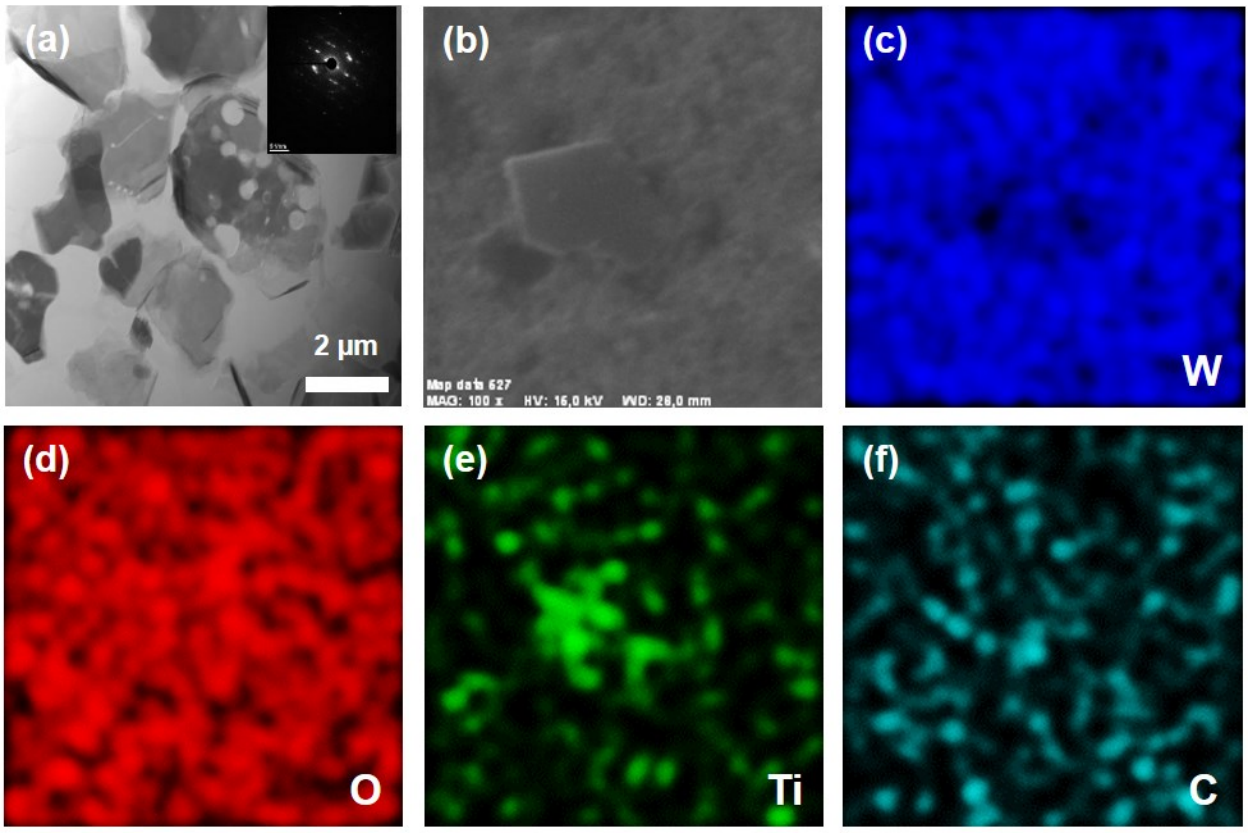

Fig. S3 (a) TEM image of $Ti_3C_2T_x$ nanosheets with SEAD pattern given in the inset; EDS mapping of $WO_3/Ti_3C_2T_x$ hybrids film with (b) SEM image of mapping area, (c) W element, (d) O element, (e) Ti element, and (f) C element.

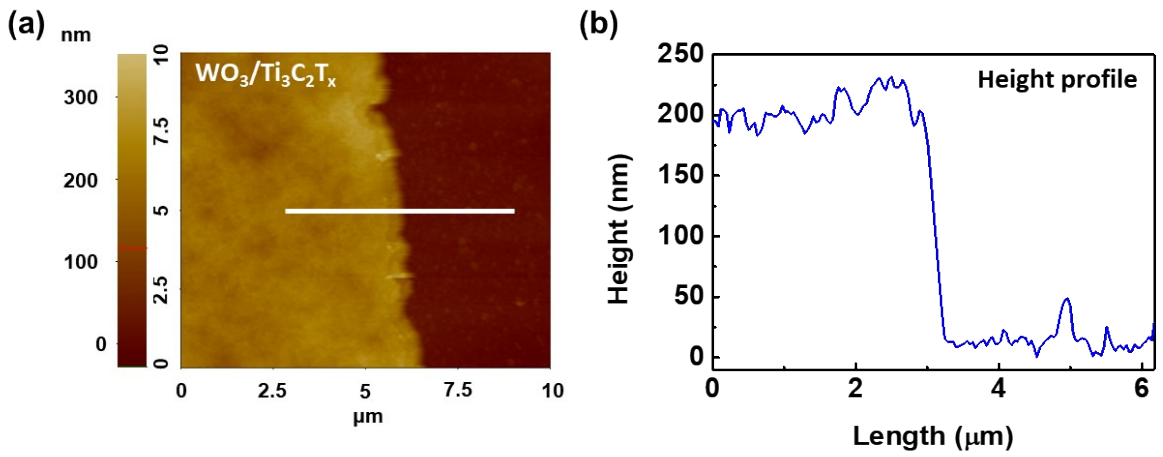

Fig. S4 (a) AFM image of $WO_3/Ti_3C_2T_x$ hybrids on ITO glass and (b) height profile of the identified line on the AFM image.

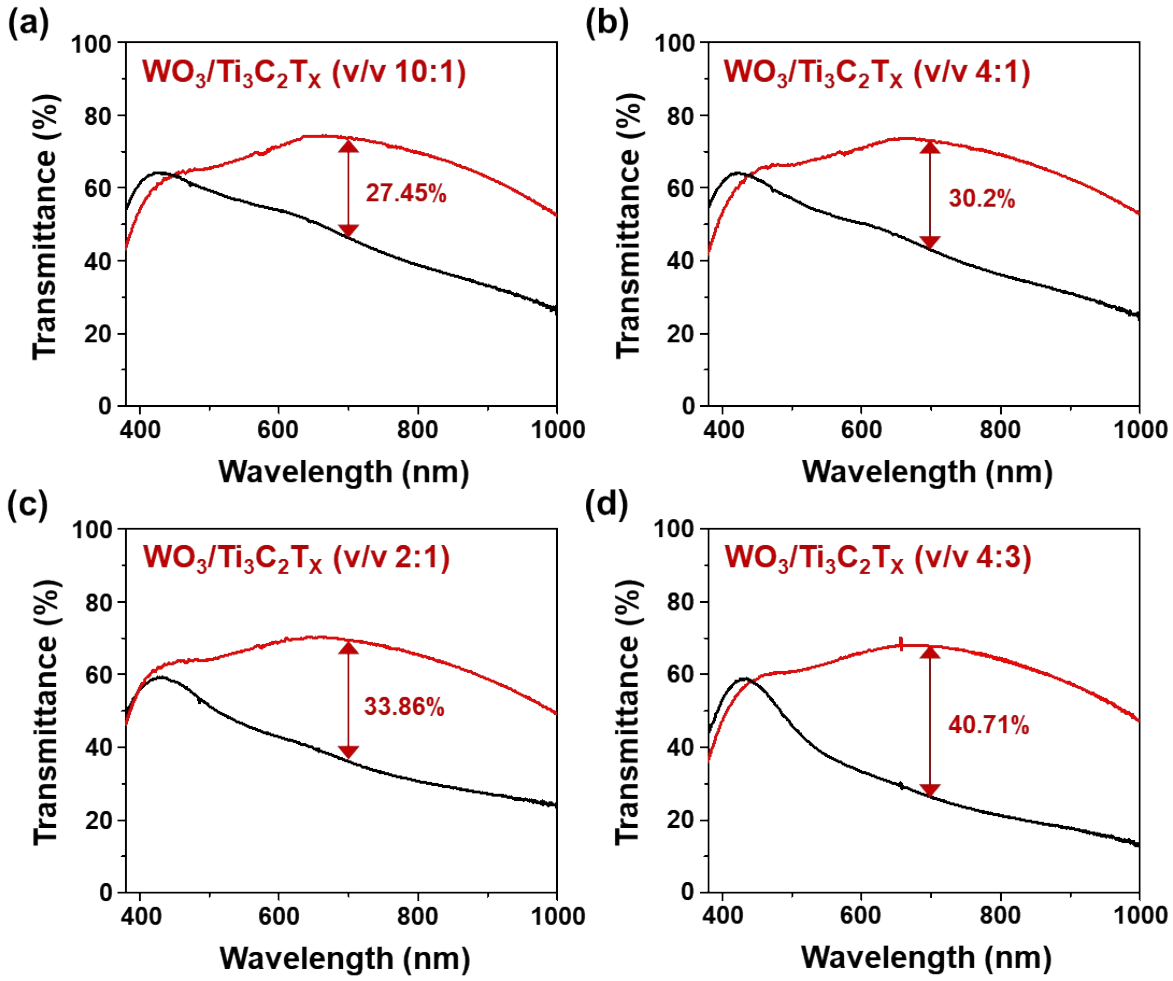

Fig. S5 Optical transmittance spectra of devices based on (a) $WO_3/Ti_3C_2T_x$ (v/v 10:1), (b) $WO_3/Ti_3C_2T_x$ (v/v 4:1), (c) $WO_3/Ti_3C_2T_x$ (v/v 2:1), (d) $WO_3/Ti_3C_2T_x$ (v/v 4:3).

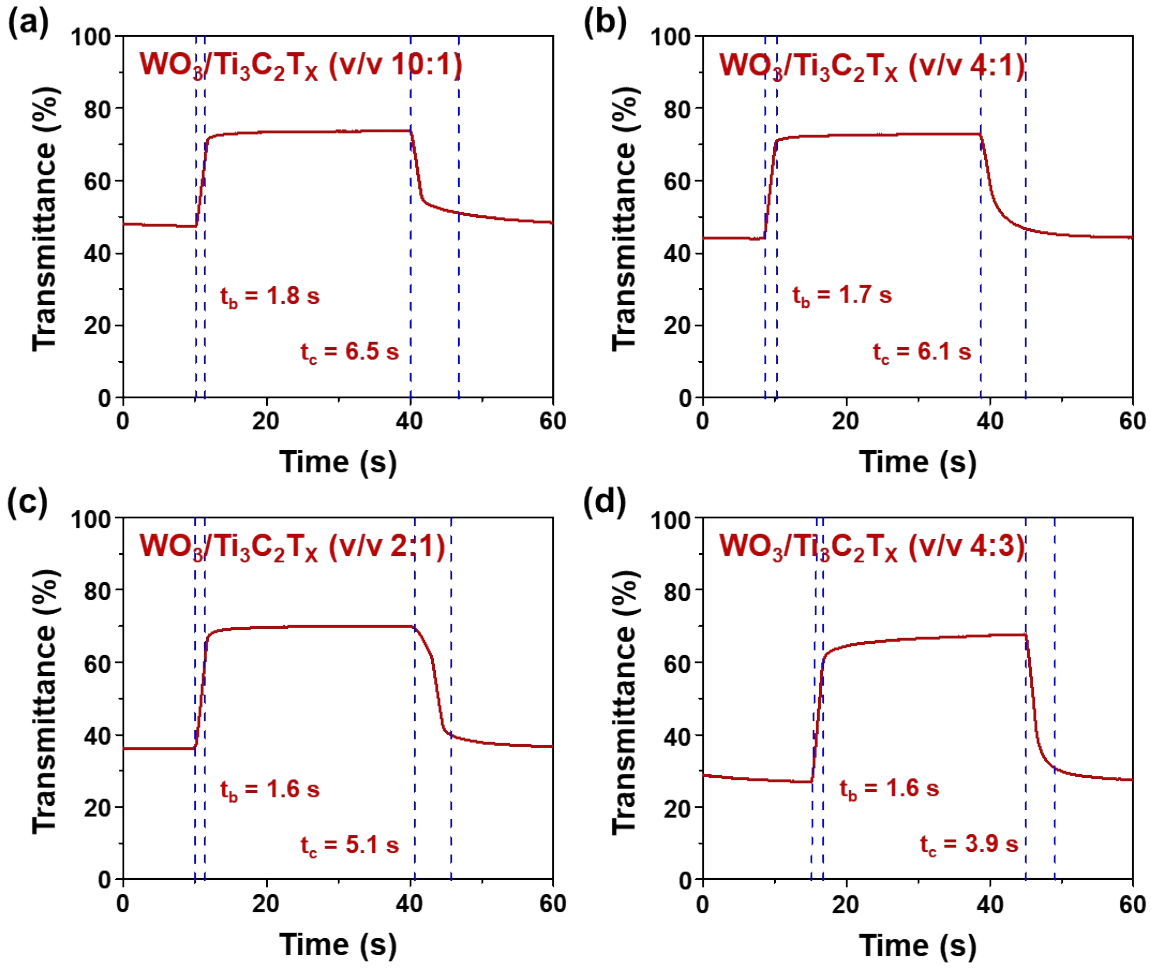

Fig. S6 EC switching kinetics of devices based on (a) $WO_3/Ti_3C_2T_x$ (v/v 10:1), (b) $WO_3/Ti_3C_2T_x$ (v/v 4:1), (c) $WO_3/Ti_3C_2T_x$ (v/v 2:1), (d) $WO_3/Ti_3C_2T_x$ (v/v 4:3) at a wavelength of 700 nm.

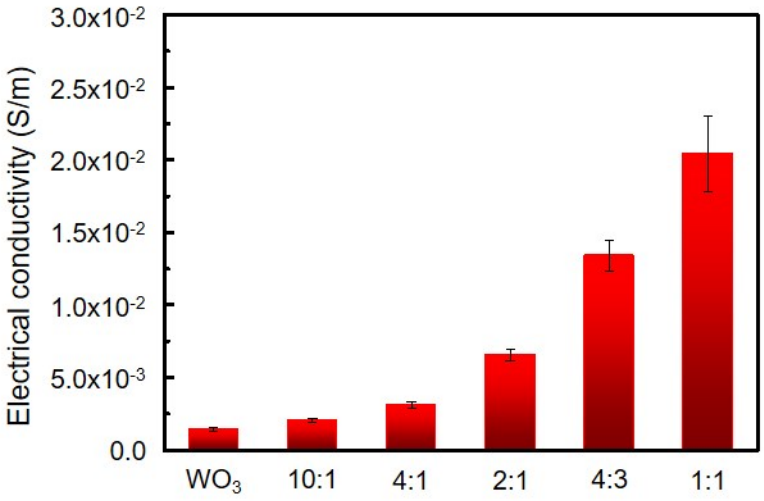

Fig. S7 Electrical conductivity of WO_3 and $WO_3/Ti_3C_2T_x$ hybrids films with various v/v ratio.

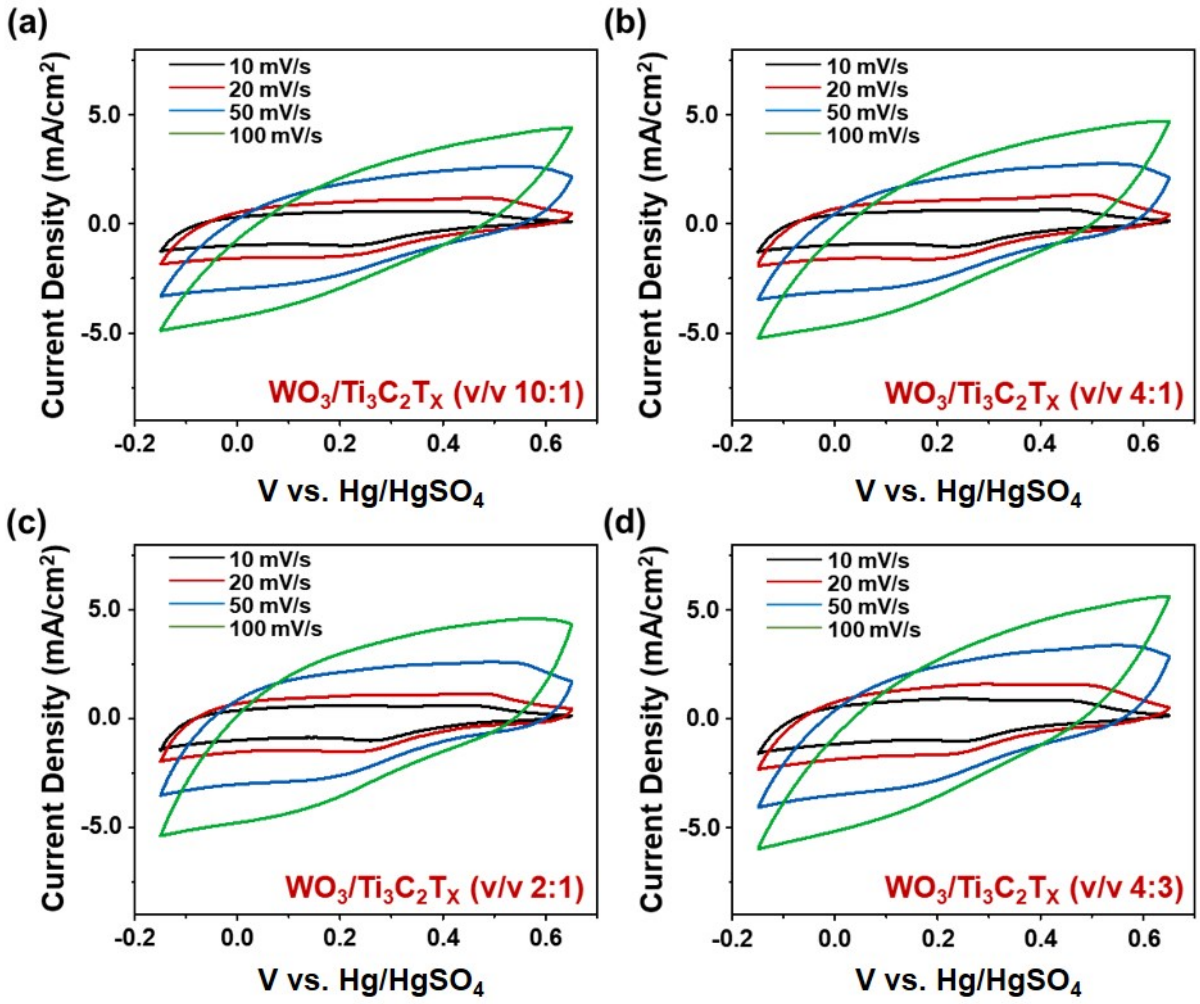

Fig. S8 CV curves of (a) $WO_3/Ti_3C_2T_x$ (v/v 10:1), (b) $WO_3/Ti_3C_2T_x$ (v/v 4:1), (c) $WO_3/Ti_3C_2T_x$ (v/v 2:1), (d) $WO_3/Ti_3C_2T_x$ (v/v 4:3) with different scan rates.

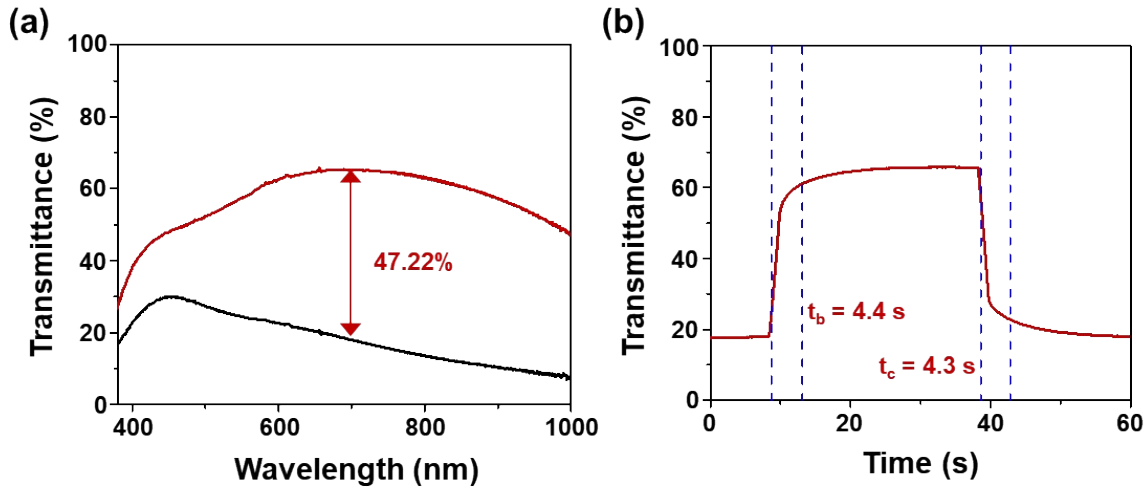

Fig. S9 (a) Optical transmittance spectrum in bleaching and coloration, (b) EC switching kinetics of a flexible EC device (5 cm x 5 cm) based on $WO_3/Ti_3C_2T_x$ hybrids.

References

1 O. Bouvard, A. Krammer, A. Schüler, *Surf. Interface Anal.*, 2016, **48**, 660-663.

2 Y. Wang, Y. Li, Z. Qiu, X. Wu, P. Zhou, T. Zhou, J. Zhao, Z. Miao, J. Zhou, S. Zhuo, *J. Mater. Chem. A*, 2018, **6**, 11189-11197.

3 Q. Zhang, J. Teng, G. Zou, Q. Peng, Q. Du, T. Jiao, J. Xiang, *Nanoscale*, 2016, **8**, 7085-7093.

4 A. Ali, K. Hantanasirisakul, A. Abdala, P. Urbankowski, M.-Q. Zhao, B. Anasori, Y. Gogotsi, B. Aïssa, K.A. Mahmoud, *Langmuir*, 2018, **34**, 11325-11334.

5 C. Shen, L. Wang, A. Zhou, B. Wang, X. Wang, W. Lian, Q. Hu, G. Qin, X. Liu, *Nanomaterials*, 2018, **8**, 80.

6 Y. Cao, Q. Deng, Z. Liu, D. Shen, T. Wang, Q. Huang, S. Du, N. Jiang, C.-T. Lin, J. Yu, *RSC Adv.*, 2017, **7**, 20494-20501.